Quantum Monte Carlo simulations of a particle in a random potential

1997 J. Phys. A: Math. Gen. 30 1803

(http://iopscience.iop.org/0305-4470/30/6/008)

J. Phys. A: Math. Gen. **30** (1997) 1803–1816. Printed in the UK PII: S0305-4470(97)77514-0

Quantum Monte Carlo simulations of a particle in a random potential

Hsuan-Yi Chen and Yadin Y Goldschmidt†

Department of Physics and Astronomy, University of Pittsburgh, Pittsburgh, PA 15260, USA

Received 28 August 1996, in final form 13 November 1996

Abstract. In this paper we carry out quantum Monte Carlo simulations of a quantum particle in a one-dimensional random potential (plus a fixed harmonic potential) at a finite temperature. This is the simplest model of an interface in a disordered medium and may also pertain to an electron in a dirty metal. We compare with previous analytical results, and also derive an expression for the sample-to-sample fluctuations of the mean square displacement from the origin which is a measure of the glassiness of the system. This quantity as well as the mean square displacement of the particle are measured in the simulation. The similarity to the quantum spin glass in a transverse field is noted. The effect of quantum fluctuations on the glassy behaviour is discussed.

1. Introduction

The problem of a quantum spin glass in a transverse field was recently at the centre of theoretical and experimental interest [1–5]. In particular the question of the interplay between glassy behaviour and quantum fluctuations and the properties of the quantum transition at zero temperature were the subject of several investigations, both for the case of the infinite-ranged spin glass and more realistic three-dimensional models.

A simpler model which catches many of the essential features of the (classical) spin glass problem is that of a directed manifold in a random medium [6–10]. An even higher simplification occurs for the case of a zero-dimensional manifold, which is equivalent to a particle in a random potential (which is localized by an additional fixed harmonic potential) [11–16]. This model has been found to require a (infinite-step) Parisi-type solution when the random potential has long-range correlations [13]. For a random potential with short-ranged correlations a one-step replica-symmetry-breaking (RSB) solution has been found [9, 15, 16]. A single particle in one dimension does not have a sharp transition into a glassy phase. But in infinite dimensions it does. It turns out that the analytical solution which utilizes the variational approximation, still possess a sharp transition at finite dimensions (including one dimension). This occurs since the replica symmetric (RS) is not able to capture the glassy features of the systems once they become strong enough, and gives rise to unphysical results, such as a non-monotonic mean square displacement of the particle from the origin as a function of the temperature. Below a certain temperature the RSB solution yields a much better physical result, and in particular the correct non-analytic behaviour at $T = 0$ as a function of the strength of the random potential in agreement with an Imry–Ma-type argument [15]. One should notice though, that the transition which has been found for a

† On sabbatical leave at the Weizmann Institute of Science, Rehovot, Israel.

0305-4470/97/061803+14$19.50

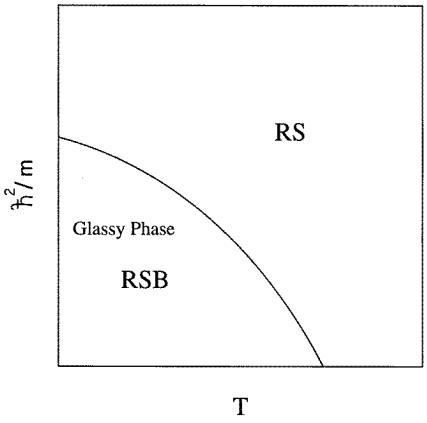

Figure 1. Schematic phase diagram of a quantum particle in a random potential plus an harmonic potential, as obtained from the variational calculation derived in I.

particle in a random potential is of the Almeida–Thouless-type [17, 18] in the sense that it is associated with a RS–RSB transition but not with an order–disorder (spin-glass-like) transition.

The success of the variational treatment of a classical particle in a random potential, led one of us recently [19, 20] to investigate a quantum analogue, i.e. to turn on $\hbar$ and consider the effect of quantum fluctuations, e.g. tunnelling on the glassy behaviour of the particle. This was suggested by the recent theoretical treatment of the quantum spin glass in a transverse field [1, 4].

Analytically we have found a glassy phase characterized by RSB, which is destroyed by the quantum fluctuations for strong enough $\hbar$, or alternatively for small enough m, which is the particle's mass. The variable $\hbar^2/m$ plays the role of the transverse field in the quantum spin glass problem. A schematic phase diagram is depicted in figure 1. The full details of the analytical investigation are given in [20], hereafter referred to as I.

Recently [21] one of us used the model of a particle in two spatial dimensions under the influence of a harmonic and a quenched random potential to describe the melting transition of the flux lattice in high-temperature superconductors with columnar disorder. The so-called cage model was originally introduced by Nelson and Vinokur [22]. In this model a single flux line is represented by the world line of a quantum particle. The influence of neighbouring flux lines is taken effectively as the cage harmonic potential. The magnitude of $\hbar$ is determined by the size of the system along the z-axis and the value of the temperature. This shows the usefulness of the toy model to other physical systems of interest.

Our aim in this paper is two-fold. First, we carried out a quantum Monte Carlo simulation of the system in one dimension in order to compare them with the analytical results obtained in I for the mean square displacement. Secondly, since both the random potential and the quantum fluctuations increase the mean square displacement, this quantity by itself is not enough to give a clear picture concerning the strength of the glassy behaviour of the system. Hence, we have measured in the simulation, and also calculated analytically the sample-to-sample fluctuation of $\langle x^2 \rangle$, which shows that the glassy behaviour of the system diminishes as the quantum fluctuation increases until the eventual termination of the glassy phase for strong enough $\hbar^2/m$. This decline in the sample-to-sample fluctuations is a gradual effect, which analytically culminates in the transition from an RSB solution to a RS solution. As mentioned previously, in a simulation which is carried out in one dimension, we do not expect to observe any sharp transitions. The trapping of the particle in deep local minima of the random potential gives rise to a sticky behaviour—i.e. a freezing of the

mean square displacement from the origin. This effect is countered by tunnelling among the different minima which enables the particle to escape from a local minima and thus diminishes the glassy behaviour.

In the next section we define the model. In section 3 we review some of the results obtained in I and obtain a new analytic result for the sample-to-sample fluctuations of the mean square displacement of the particle from the origin. In section 4, we describe the details of the quantum Monte Carlo (QMC) simulation. Section 5 is devoted to a discussion of the results and a summary. A comparison is made between the simulation and the theoretical results obtained in I and in section 3. In the appendix we give some further details of the calculation presented in section 3.

2. The model

The partition function for a particle at finite temperature $T = 1/k_B\beta$, subject to a harmonic potential and a random potential V, is given by the functional integral [23]:

$$Z(U) = \int_{\boldsymbol{x}(0)=\boldsymbol{x}(U)} [d\boldsymbol{x}] \exp\left\{ -\frac{1}{\bar{h}} \int_0^U \left[\frac{m\dot{\boldsymbol{x}}(u)^2}{2} + \frac{\mu \boldsymbol{x}(u)^2}{2} + V(\boldsymbol{x}(u)) \right] \mathrm{d}u \right\} \tag{2.1}$$

where $\boldsymbol{x}$ is an N-dimensional vector (N is the number of spatial dimensions), and $U = \beta\bar{h}$. The variable u has dimensions of time and is often referred to as the Trotter dimension. We observe that the trajectory $\boldsymbol{x}(u)$ forms a closed path. In this paper we are concerned with a random quenched potential $V(x)$, which is Gaussian distributed. This means that the probability for a given realization of the potential is given by:

$$P(V(x)) = C \exp\left(-\int \mathrm{d}x\, \mathrm{d}x' V(x) \Delta(x - x') V(x') \right) \tag{2.2}$$

with some known function $\Delta(x-x')$. It is thus sufficient to know only the first two moments of the distribution, namely

$$\langle V(\boldsymbol{x}) \rangle_R = 0 \qquad \langle V(\boldsymbol{x}) V(\boldsymbol{x}') \rangle_R = -N f\left(\frac{(\boldsymbol{x} - \boldsymbol{x}')^2}{N} \right) \tag{2.3}$$

where the functions f and Δ are related to each other. The function f describes the correlations of the random potential. In this paper we consider two cases. One, which we call the case of long-ranged correlations of the potential, for which f is taken to decay as a power at large distances:

$$f(y) = \frac{g}{2(1-\gamma)} (a_0 + y)^{1-\gamma} \tag{2.4}$$

with $\gamma = \frac{1}{2}$. This case corresponds, in one dimension, to an interface in the random field Ising model [6, 9, 14, 15]. The parameter a_0 plays the role of a short-distance regulator for f. Another type of random potential we consider has Gaussian correlations and we refer to it as the case of short-ranged correlations. For this case, the function f is taken to decay as an exponential function at large distances:

$$f(y) = \frac{g}{2} \exp(-\tfrac{1}{2} y). \tag{2.5}$$

In the classical case it has been shown that (for $N = 1$) even when correlations fall exponentially fast, the physics is equivalent within the variational approximation to the case of random potential with power law correlations (equation (2.4)) and $\gamma = \frac{3}{2}$ at large distances [9, 15]. This fact also holds in the quantum case, as has been demonstrated in I. Thus, we will compare the results obtained in the QMC for the distribution (2.5) with results obtained in I for the case of $\gamma = \frac{3}{2}$.

3. Theoretical considerations

In paper I we investigated the problem using the replica method and the variational approximation. Here we review briefly some of the formalism and discuss the new derivation of the sample-to-sample fluctuation of the mean square displacement that is a measure of the glassiness of the system and is needed to compare with the results of the QMC simulations. Some details are deferred to the appendix. Readers who are interested only in the details of the QMC simulation can skip this section.

In the replica method variational approach the system is represented by an n-body variational Hamiltonian:

$$h_n = \frac{1}{2}\int_0^U \mathrm{d}u \sum_a [m\dot{\boldsymbol{x}}_a^2(u) + \mu \boldsymbol{x}_a^2(u)] - \frac{1}{2\overline{h}}\int_0^U \mathrm{d}u \int_0^U \mathrm{d}u' \sum_{ab} s_{ab}(u-u')\boldsymbol{x}_a(u)\cdot\boldsymbol{x}_b(u'). \tag{3.1}$$

The matrix $s_{ab}(u-u')$ is determined by extremizing the variational free energy which is given by:

$$n\beta\langle F\rangle_R/N = \langle \mathcal{H}_n - h_n\rangle_{h_n}/\overline{h} - \ln\int [\mathrm{d}x]\mathrm{e}^{-h_n/\overline{h}}. \tag{3.2}$$

Here $\mathcal{H}_n$ is the exact n-body Hamiltonian. The limit $n \to 0$ has to be taken at the end.

The propagator associated with h_n is given in frequency space

$$G_{ab}(\omega) \equiv ([(m\omega^2+\mu)\mathbf{1} - \tilde{s}(\omega)]^{-1})_{ab}. \tag{3.3}$$

ω is the frequency conjugate to the Trotter time variable u, and takes the values:

$$\omega_l = \frac{2\pi}{U}l \qquad l = 0, \pm 1, \pm 2, \ldots \tag{3.4}$$

and the matrix $\tilde{s}_{ab}(\omega)$ is related to $s_{ab}(u)$ by:

$$s_{ab}(\zeta) = \frac{1}{\beta}\sum_{l=-\infty}^{\infty} \exp(-\mathrm{i}\omega_l\zeta)\tilde{s}_{ab}(\omega_l). \tag{3.5}$$

We have found a self-consistent solution to the variational equations where only the diagonal elements of the matrix s_{ab} are 'time' dependent, and the off-diagonal elements are independent of the Trotter time. Thus

$$\tilde{s}_{aa}(\omega) = \tilde{s}_d(\omega) \tag{3.6}$$

$$\tilde{s}_{ab}(\omega, z) \leftrightarrow \tilde{s}(z)\delta_{\omega,0} \qquad a \neq b \tag{3.7}$$

where the Parisi parameter $0 < z < 1$ labels the 'distance' between replicas indices ab. A similar behaviour follows for the propagator matrix $G_{ab}(\omega)$ with a similar notation $G_d(\omega)$ and $G(z)$. (These are the same as the quantities $\tilde{r}_d(\omega)$ and $\tilde{r}(z)$ used in I.)

The mean square displacement from the origin is given by:

$$\langle\langle \boldsymbol{x}^2\rangle\rangle_R/N = \frac{1}{\beta}\sum_{k=-\infty}^{\infty} G_d(\omega_k). \tag{3.8}$$

This quantity was evaluated in I.

The sample-to-sample fluctuation of $\langle \boldsymbol{x}^2\rangle$ is a measure of the glassiness of the system. In the replica approach together with the variational approximation, this quantity is represented by

$$\langle\langle \boldsymbol{x}^2\rangle^2\rangle_R - \langle\langle \boldsymbol{x}^2\rangle\rangle_R^2 = \langle \boldsymbol{x}_a^2\boldsymbol{x}_b^2\rangle_{h_n} - \langle \boldsymbol{x}_a^2\rangle_{h_n}^2 \tag{3.9}$$

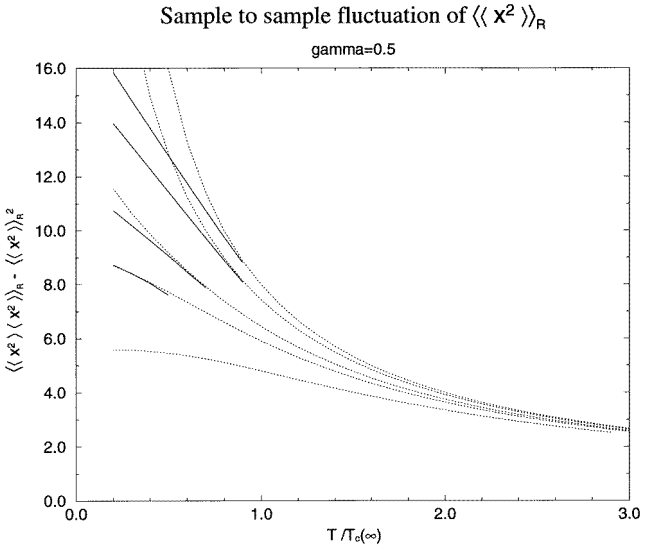

Figure 2. Plot of sample-to-sample fluctuations of $\langle\langle \boldsymbol{x}^2\rangle\rangle_R$ for long-ranged correlated disorder from numerical solution. Broken curves are solutions assuming replica symmetry. Full curves are RSB solutions. From top to bottom: $\kappa = 100$, 1.0, 0.3, 0.2, 0.1.

where a and b are indices for replicas. Following the notation we used in I, the sample-to-sample fluctuation of the mean square displacement becomes:

$$\frac{1}{N^2}(\langle\langle \boldsymbol{x}^2\rangle^2\rangle_R - \langle\langle \boldsymbol{x}^2\rangle\rangle_R^{\,2}) = \frac{2}{N\beta^2}\int_0^1 G^2(z)\,\mathrm{d}z. \tag{3.10}$$

For a particle in N dimensions it is self-averaging in the large N limit but not for $N = 1$. The degree of non-self-averaging is a measure of the glassy behaviour of the system.

In the appendix we give details of the numerical evaluation of the sample-to-sample fluctuation of $\langle\langle \boldsymbol{x}^2\rangle\rangle$ both in the replica symmetric and in the RSB phases. The calculation is done both for the case of continuous RSB which occurs for a random potential with long ranged correlations, and for the case of short-ranged correlated potential where there is a one-step RSB. The results are depicted in figures 2 and 3, respectively. We observe that the glassiness of the system increases with decreasing temperature, but decreases with increasing $\hbar^2/m \equiv 1/\kappa$. Recall that the transition temperature $T_c(\kappa)$ between the RS and RSB phases decrease with decreasing κ as was obtained in I.

Another quantity that could also be used as a measure for the glassiness of the system, but we did not measure in the QMC simulation, is the sample-to-sample fluctuation of the susceptibility,

$$\chi = \frac{1}{N}(\langle \boldsymbol{x}^2\rangle - \langle \boldsymbol{x}\rangle^2) \tag{3.11}$$

which is given by:

$$\langle\chi^2\rangle_R - \langle\chi\rangle_R^2 = \frac{1}{3\beta^2}\left(1+\frac{2}{N}\right)\left[\int_0^1 \mathrm{d}z\, G^2(z) - \left(\int_0^1 \mathrm{d}z\, G(z)\right)^2\right]. \tag{3.12}$$

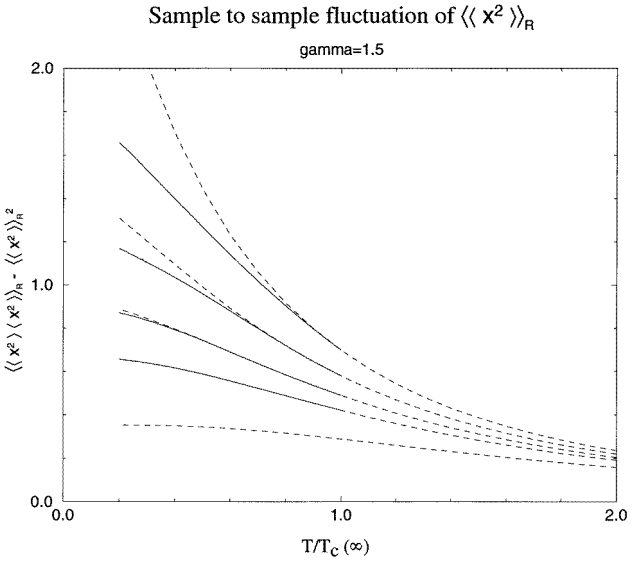

Figure 3. Plot of sample-to-sample fluctuations of $\langle \boldsymbol{x}^2 \rangle$ for short-ranged correlated disorder from the numerical solution. Broken curves are solutions assuming replica symmetry. Full curves are one-step RSB solutions. From top to bottom: $\kappa = 100$, 6, 3, 2, 1.

4. Numerical simulations

We applied the path integral Monte Carlo method (PIMC) in one space dimension to calculate the relevant physical quantities that we are interested in. The partition function of this system at a given temperature is given by

$$Z(T) = \int_{\boldsymbol{x}(0)=\boldsymbol{x}}^{\boldsymbol{x}(U)=\boldsymbol{x}'} [\mathrm{d}\boldsymbol{x}] \exp\left\{ -\frac{1}{\hbar} \int_0^U \left[\frac{m\dot{\boldsymbol{x}}(u)^2}{2} + \frac{\mu \boldsymbol{x}(u)^2}{2} + V(\boldsymbol{x}(u)) \right] \mathrm{d}u \right\}. \tag{4.1}$$

We discretize $x(\tau)$ into $M+1$ points with $x(1)$ equal to $x(M+1)$. The partition function now becomes an M-dimensional ordinary integral, i.e.

$$Z(T) = \int \prod_{i=1}^{M} \frac{\mathrm{d}x_i}{A} \exp\left[-\sum_{j=1}^{M} \varepsilon \left[\frac{m}{2} \left(\frac{(x_{j+1} - x_j)}{\varepsilon} \right)^2 + \frac{\mu}{2} x_j^2 + V(x_j) \right] \right] \tag{4.2}$$

where $\varepsilon = U/M$, $A = \sqrt{2\pi\hbar\varepsilon/m}$. In this way we are able to apply the Metropolis method to perform the integration for the partition function.

In this form the partition function of a quantum particle is similar to the classical Boltzmann distribution of a polymer ring with M beads under the influence of an applied harmonic potential and a random potential. The beads have a harmonic spring interaction between neighbouring beads and in addition each bead feels a combination of a harmonic (with respect to the origin) and a random local potential. This gives us an intuitive picture of the simulation. In the simulation one attempts to move each bead in its own turn and one checks if the 'energy' (minus the argument of the exponential) decreases or increases. Then one actually moves the bead in accordance to a detailed balance algorithm, e.g. the Metropolis algorithm.

The problem of doing PIMC comes from the fact that for small ε (or large M) the beads are not easy to move due to a very large spring constant, thus the acceptance rate is low

for a reasonable size move and convergence is not easy to achieve in a reasonable time. For this reason many efforts have been made to circumvent the problem [24–27]. We use the normal mode PIMC to perform the calculation [24]. In our program the motion of the 'beads' includes 2 parts, i.e.

(1) Microscopic movement: we attempt to change the value of each x_i individually. We put $x_i' = x_i + \mathrm{d}x$ and decide whether x_i should change or not.

(2) Global movement: we consider all x_i's together as a set, and consider

$$x_i' = x_i + a_0 + \sum_{q=1}^{q_c} a_q \sin\left(2\pi q \frac{\mathrm{i}-1}{M}\right) \qquad \forall i = 1 \ldots M. \tag{4.3}$$

In our simulation the total number of points on the 'time' axis are chosen such that more points are used for the small κ regime. The numbers range from 7 to 16. Although this is not a large number, results from simulations we carried out for a simple harmonic oscillator give rather small errors. This gives us confidence that in the presence of random potentials the small number of points in the Trotter time dimension will also give us a small error in comparison with the statistical error which comes from the small number of samples of random potentials. Since this is not a very large number of points we found it sufficient to include only the zeroth and first normal modes, i.e. we choose $q_c = 1$, and then decide whether they move or not. The magnitude of $\mathrm{d}x$ and the a_i's are chosen so that the acceptance ratio is approximately 0.5. The parameters a_0, a_1, and the size of microscopic movement, $\mathrm{d}x$, are listed in table 1 at the end of this section.

We have generated two kinds of random potentials: A random potential with long-range correlation, characterized by $\gamma = \frac{1}{2}$ and a random potential with short-range correlation which decay like a Gaussian. Within the framework of the variational approximation such a potential is equivalent to a random potential with power law correlations that are characterized by an index $\gamma = \frac{3}{2}$.

For the case of a long-range correlation, we have generated that $K = 6000$ uncorrelated random numbers $h_1 \ldots h_K$ with a Gaussian distribution. We then constructed the variables $V_0 \ldots V_K$ by:

$$V_i = \text{constant}\left(\sum_{j=0}^{i} h_j - \sum_{j=i}^{K} h_j\right) \tag{4.4}$$

and placed them on one-dimensional lattice with a lattice constant chosen to be 0.01. The random potential generated in this way has correlation

$$\langle V_i V_j \rangle_R = -\text{constant}|i-j| + C \tag{4.5}$$

where C is a constant independent of i, j. The free energy depends trivially on C but $\langle\langle \boldsymbol{x}^2 \rangle\rangle_R$ is independent of C as has been mentioned in equation (2) of [13]. In this way a random potential with long-range correlation is generated. These 6000 numbers have long-ranged correlations with $\gamma = \frac{1}{2}$.

We now discuss the procedure to generate a random potential with short range correlations. From the fact that random potentials with correlation

$$\langle V(x_1) V(x_2) \rangle_R \propto \exp\left(-\frac{a}{2}(x_1 - x_2)^2\right) \tag{4.6}$$

in configuration space have correlations in momentum space with the following form

$$\langle V_{k_1} V_{k_2} \rangle_R \propto \delta(k_1 + k_2) \exp(-{k_1}^2/2a) \tag{4.7}$$

we generated random numbers with a proper distribution in momentum space and fast Fourier transformed them by a standard Fortran subroutine [28] to get random numbers

with a Gaussian *correlation*. We put 4000 of them on lattice sites with a lattice constant of 0.005. These constitute a random potential with short (Gaussian) correlations. In both long- and short-ranged disorder, we discretize the x-direction such that the lattice is about 2 orders of magnitude smaller than $\langle\langle \boldsymbol{x}^2 \rangle\rangle_R$.

Another difficulty is that in the low-temperature regime the relaxation time of the system is very long because the phase space of the system is separated by high free energy barriers and it is difficult to get reliable results within a reasonable computer time. The standard approach of doing a simulation in these systems is the simulated annealing approach, and in addition to using this method we also used a modified version of the global movement algorithm to speed up the dynamics.

We started our simulation from the high temperature regime ($T = 3T_c(\infty)$ for long-range correlation case and $T = 2T_c(\infty)$ for short-range correlation case). We then lowered the temperature in steps of $1T_c(\infty)$ when $T > T_c(\infty)$. For $T < T_c(\infty)$ we lowered the temperature by $\delta T = 0.1T_c(\infty)$ at a time and performed thermal averages for every $0.2T_c(\infty)$. The lowest temperature of our simulation was set to be $0.2T_c(\infty)$. In addition, we attempted two different size (zeroth mode) global movements in each sweep, of magnitudes a_0 and a_0' respectively. Generally, we choose one of these parameters, say a_0, to be much bigger than the other (but such the acceptance rate will not fall below 0.01) in order that the particle will get a chance to occasionally escape from deep wells which correspond to metastable minima. We have performed the simulation for different given random potentials with thermalization sweeps in the range of 30 000–200 000 and averaged over 200 000–2 000 000 MC steps and only a very small difference have been found. When taking data we have chosen the number of thermalization sweeps to be 50 000 for all cases and averaged over 200 000–400 000 steps with more steps for lower temperatures.

Table 1 gives an example for the parameters we have chosen for the simulation in the case of long-ranged correlated potential.

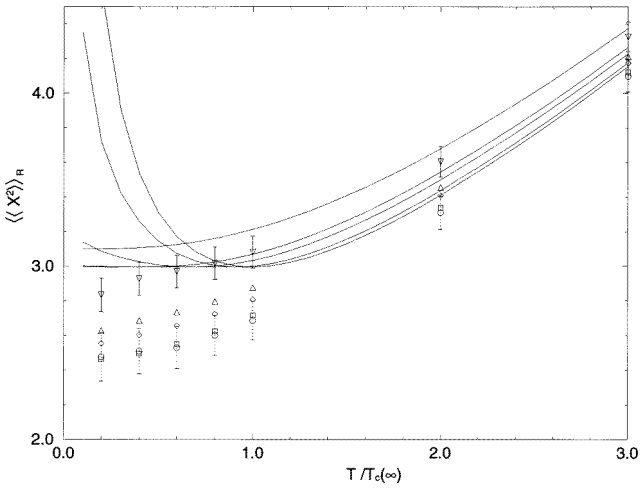

Figure 4. Plot of $\langle\langle \boldsymbol{x}^2 \rangle\rangle_R$ versus $T/T_c(\infty)$ for long-ranged correlated disorder. Full curves are numerical solutions, obtained in I, assuming replica symmetry. From top to bottom: $\kappa = 0.1, 0.2, 0.3, 1.0, 100$. Data points are Monte Carlo simulations for $\kappa = 100$ (circles), $\kappa = 1.0$ (squares), $\kappa = 0.3$ (diamonds), $\kappa = 0.2$ (up triangles), and $\kappa = 0.1$ (down triangles). Each point is averaged over 2000 samples. Error bars indicate the statistical errors for the cases of $\kappa = 100$ (dotted line) and $\kappa = 0.1$ (full line).

Table 1. Example of different parameters in the QMC for the long-ranged correlated potential.

t	dx	a_0	a_0'	a_1
$\kappa = 100$				
3.0	0.02	2.30	2.0	0.03
2.0	0.02	2.00	1.3	0.04
1.0	0.03	1.70	0.4	0.04
0.9	0.03	1.50	0.4	0.04
0.8	0.03	1.20	0.3	0.05
0.7	0.03	1.00	0.2	0.05
0.6	0.04	0.90	0.15	0.06
0.5	0.04	0.90	0.12	0.06
0.4	0.05	0.80	0.10	0.07
0.3	0.05	0.80	0.09	0.07
0.2	0.06	0.70	0.08	0.08
$\kappa = 0.2$				
3.0	0.30	1.45	1.45	0.80
2.0	0.30	1.05	1.05	0.90
1.0	0.35	1.00	1.00	0.95
0.9	0.37	0.95	0.80	0.85
0.8	0.48	0.90	0.70	0.85
0.7	0.59	0.90	0.60	0.85
0.6	0.60	0.85	0.50	0.80
0.5	0.71	0.85	0.45	0.80
0.4	0.82	0.80	0.40	0.80
0.3	0.82	0.80	0.35	0.66
0.2	0.82	0.70	0.20	0.45

5. Results and discussion

The mean square displacement of the particle as well as the sample-to-sample fluctuations of the mean square displacement are calculated in our simulation, and all data points are averaged over 2000 samples of the random potential.

For the classical case, previous numerical results for the long-range case, were reported by [13] for the long-ranged case and also by [15] for both the short- and long-ranged cases. They did not perform Monte Carlo simulations, but used the fact that in the classical case instead of a path integral one has to evaluate a simple integral for each realization of the random potential. For large $\kappa (= 100)$, where the results should reduce to the classical case, we have checked our results for the mean square displacement against the results of [13, 15], and the agreement is quite good, taking into account the fact that we have averaged over 2000 realizations of the disordered versus 10 000 in [15] and 40 000 in [13]. In doing a PIMC we did not have enough computer time to average over a larger number of realizations.

In figure 4 we show the results of the Monte Carlo simulations for the mean square displacement, for the case of long-ranged correlated potential. For comparison we show the results obtain from the analytical solution reported in I. As in the classical case we observe that when quantum effects are turned on, the RS symmetric solution gives an unphysical result below $T_c(\kappa)$, down to a certain critical κ. The RSB solution gives rise to a flat behaviour of $\langle\langle x^2 \rangle\rangle_R$ below $T_c(\kappa)$. The actual results of the QMC show that the function is indeed monotonic, but no sharp transition is observed, and it continues to decrease at all temperatures. A sharp transition is only expected at $N = \infty$, whereas the simulation has

Table 2. Example of $\langle\langle x^2\rangle\rangle_R$ from two sets of 1000 realizations of the long-ranged correlated random potential in the QMC.

t	$\langle\langle x^2\rangle\rangle_R$, first 1000 samples	$\langle\langle x^2\rangle\rangle_R$, second 1000 samples
$\kappa = 1.0$		
3.0	4.185	4.058
2.0	3.396	3.281
1.0	2.767	2.662
0.8	2.672	2.574
0.6	2.601	2.497
0.4	2.552	2.437
0.2	2.519	2.404
$\kappa = 0.3$		
3.0	4.237	4.112
2.0	3.465	3.352
1.0	2.857	2.755
0.8	2.774	2.670
0.6	2.701	2.603
0.4	2.654	2.552
0.2	2.610	2.498
$\kappa = 0.2$		
3.0	4.276	4.148
2.0	3.514	3.402
1.0	2.925	2.824
0.8	2.846	2.745
0.6	2.784	2.683
0.4	2.734	2.636
0.2	2.677	2.577

been carried out at $N = 1$, where N is the number of spatial dimensions. The variational approximation also gives rise to a sharp transition at all dimensions, much like the large N result. As κ decreases, tunnelling increases and the glassiness of the system decreases as the particle is able to tunnel across potential barriers. This is evident in the analytical solution by the decrease of $T_c(\kappa)$ with decreasing κ, until there is no longer any transition.

In this simulation we found that the statistical errors are dominated by the sample-to-sample fluctuations of $\langle x^2\rangle$ (the discussion of this quantity is in the next paragraph). For this reason, the error bars in figure 4 are given by

$$\pm 2(\langle\langle x^2\rangle\langle x^2\rangle\rangle_R - \langle\langle x^2\rangle\rangle_R^2)^{1/2}/\sqrt{(\text{number of samples})} \tag{5.1}$$

with the number of samples being 2000 in our case. We give only the error bars for the case of $\kappa = 100$ and $\kappa = 0.1$ otherwise the figure would become too messy. The error bars increase with increasing κ. Also, in table 2 we give the value of $\langle\langle x^2\rangle\rangle_R$ for the first and second 1000 samples for $\kappa = 0.2$, 0.3, and 1.0. We found that all the values of $\langle\langle x^2\rangle\rangle_R$ are within the error bars for those values of κ which is very reasonable.

What is the signature of this effect in the simulations? In order to see this effect we measured the sample-to-sample fluctuations of $\langle x^2\rangle$. This is a direct measure for the glassiness of the system. In figure 5 we depict the sample-to-sample fluctuation of $\langle x^2\rangle$ and observe that for small enough κ the function becomes flat with decreasing temperature which signals the fact that quantum effects wipe out the glassy behaviour. This figure is to be compared with the figure 2 obtained from the variational approximation.

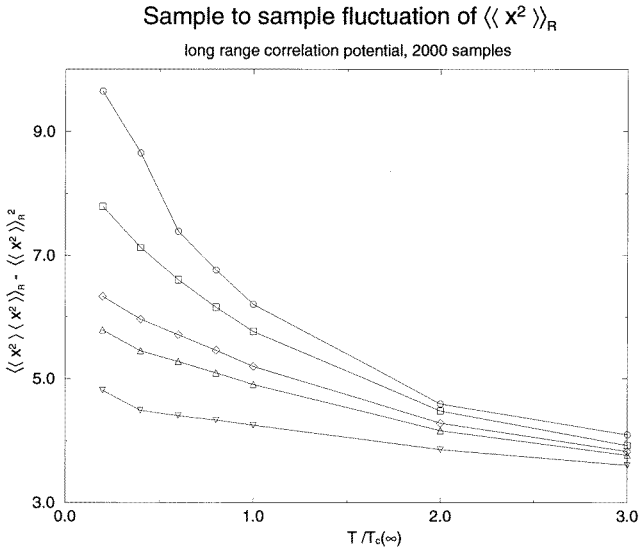

Figure 5. Plot of sample-to-sample fluctuations of $\langle \boldsymbol{x}^2 \rangle$ for long-ranged correlated disorder from Monte Carlo simulations. Data points are for $\kappa = 100$ (circles), $\kappa = 1.0$ (squares), $\kappa = 0.3$ (diamonds), $\kappa = 0.2$ (up triangles), and $\kappa = 0.1$ (down triangles). Each point is averaged over 2000 samples.

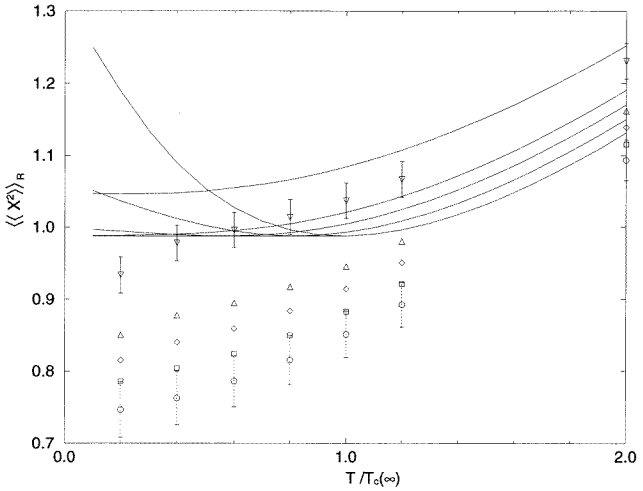

Figure 6. Plot of $\langle\langle \boldsymbol{x}^2 \rangle\rangle_R$ versus $T/T_c(\infty)$ for short-ranged correlated disorder. Full curves are numerical solutions, obtained in I, assuming replica symmetry. From top to bottom: $\kappa = 1, 2, 3, 6, 100$. Data points are Monte Carlo simulations for $\kappa = 100$ (circles), $\kappa = 6$ (squares), $\kappa = 3$ (diamonds), $\kappa = 2$ (up triangles), $\kappa = 1$ (down triangles). Each point is averaged over 2000 samples. Error bars indicate the statistical errors for the cases of $\kappa = 100$ (dotted bar) and $\kappa = 1$ (full bar).

We also have to notice that the large sample-to-sample fluctuation of $\langle \boldsymbol{x}^2 \rangle$ in the low-temperature regime also indicates that the error bars on our graphs for $\langle \boldsymbol{x}^2 \rangle$ are relatively large in the glassy phase. In fact the uncertainty of our calculation from only 2000 samples is not enough to make a highly precise quantitative description of the behaviour of this system.

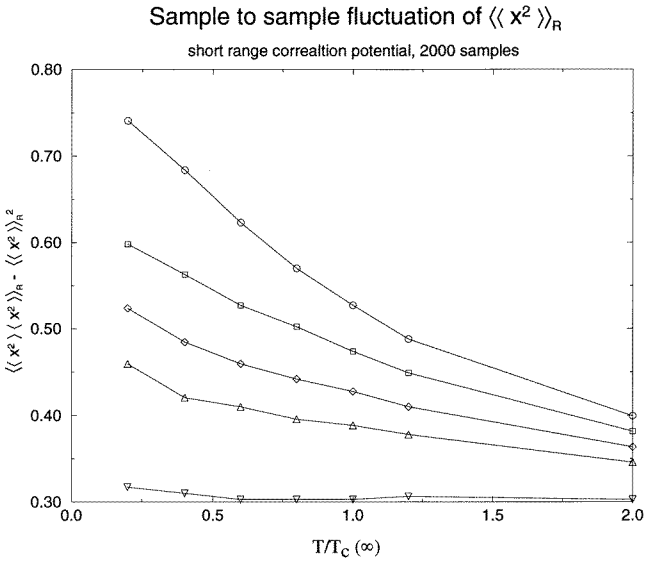

Figure 7. Plot of sample-to-sample fluctuations of $\langle \boldsymbol{x}^2 \rangle$ for short-ranged correlated disorder from Monte Carlo simulations. Data points are for $\kappa = 100$ (circles), $\kappa = 6$ (squares), $\kappa = 3$ (diamonds), $\kappa = 2$ (up triangles), $\kappa = 1$ (down triangles). Each point is averaged over 2000 samples.

Nevertheless, for a qualitative study of this system at a low temperature our simulation gives a clear picture.

Similar results were obtained for the case of short-ranged correlated potential. In figure 6 we display the PIMC results for the mean square displacement together with the results obtained in I from the analytical calculation for the RS solution. The analytical solution has been obtained for power correlations with $\gamma = \frac{3}{2}$, but from the variational approximation any faster falling correlation should give similar results.

In figure 7 we show the sample-to-sample fluctuations of $\langle \boldsymbol{x}^2 \rangle$ for the short-ranged case, as obtained from the QMC simulations to be compared with figure 3 obtained the analytical variational calculation. Again we observe the reduction of the glassiness of the system with an increase of the quantum effects.

To conclude, we observe the relatively good agreement between the QMC simulation and the results of the variational calculation. Some of the deviations are, of course, due to the variational approximation, but they are also due to the fact that in the simulation we averaged only over 2000 realizations. The results show that the sample-to-sample fluctuations of the mean square deviation of the particle from the origin are a good measure of the glassiness of the system which decreases with increasing quantum effects (increase of $\bar{h}^2/m$). Thus, the qualitative similarity with the phase diagram of the quantum spin glass in a transverse field is established.

Acknowledgments

We thank the Pittsburgh Supercomputer Center for support under grant no DMR950018P. YYG thanks the Weizmann Institute for support as a Michael Visiting Professor, where part of this work has been done.

Appendix

For the temperature range where the RS solution is valid, it has been shown in appendix B of I how to obtain the numerical solution of the self-consistent equations (4.15) and (4.16) of I. When replica symmetry is broken, in the case of long-ranged correlated potential, the equations for the self-energy matrix are given in equations (5.3)–(5.8) of I. The solution of equation (5.6) of I is obtained analytically there, and is presented in equations (5.9)–(5.11) which are reproduced below.

The off-diagonal elements parametrized by the Parisi variable z are given by:

$$\tilde{s}(z) = \begin{cases} \frac{3}{2}Az_1^2 & 0 < z < z_1 \\ \frac{3}{2}Az^2 & z_1 < z < z_2 \\ \frac{3}{2}Az_2^2 & z_2 < z < 1 \end{cases}$$

with

$$A = (\tfrac{2}{3})^3 g^2 \beta^3 \tag{A1}$$

$$z_1 = \tfrac{3}{2} g^{-2/3} \mu^{1/3} \beta^{-1} \tag{A2}$$

and z_2 is the solution of the equation

$$\tfrac{1}{2}\beta A a_R z_2^4 + z_2 - \tfrac{3}{4} = 0 \tag{A3}$$

where

$$a_R(\beta, m, \mu, g) = a_0 + b_0(\beta, \kappa, \mu, g) \tag{A4}$$

with

$$b_0(\beta, \kappa, \mu, g) = \frac{2}{\beta} \sum_{\omega \neq 0} \frac{1}{m\omega^2 + \mu - \tilde{s}_d(\omega)}. \tag{A5}$$

We integrate $\tilde{s}$ over z to obtain $\int_0^1 \mathrm{d}z\, \tilde{s}(z)$ and substitute it into equation (5.7) of I:

$$\tilde{s}_d(\omega) = \int_0^1 \mathrm{d}z\, \tilde{s}(z) - \frac{2}{\hbar} \int_0^U \mathrm{d}\zeta\, (1 - \mathrm{e}^{\mathrm{i}\omega\zeta}) f' \left(\frac{2}{\beta} \sum_{\omega' \neq 0} \frac{1 - \mathrm{e}^{-\mathrm{i}\omega'\zeta}}{m\omega'^2 + \mu - \tilde{s}_d(\omega')} \right). \tag{A6}$$

Then we have a set of nonlinear equations for $\tilde{s}_d(\omega)$'s which are solved for up to 20 non-zero Matsubara frequencies ($l = -10 \ldots 10$, in equation (3.4)). The solution is then used (utilizing equation (5.4) of I) to calculate the sample-to-sample fluctuation of $\langle \boldsymbol{x}^2 \rangle$ as given in equation (3.10), and is depicted in figure 2.

For the case of short-ranged correlations, we seek a solution with one-step replica symmetry breaking, i.e.

$$\tilde{s}(z) = \begin{cases} s_0 & 0 < z < z_c \\ s_1 & z_c < z < 1 \end{cases}$$

and hence

$$[\tilde{s}](z) = z\tilde{s}(z) - \int_0^z \mathrm{d}z\, \tilde{s}(z). \tag{A7}$$

is given by

$$[\tilde{s}](z) = \begin{cases} 0 & 0 < z < z_c \\ \Sigma & z_c < z < 1 \end{cases}$$

where $\Sigma = z_c(s_1 - s_0)$. The breaking point and the order parameters s_0, s_1 are found from maximizing the variational free energy. The equations are similar to the classical case [15], the difference between the classical and the quantum case enters again through the renormalization of the constant $a_0 \to a_R = a_0 + b_0$ which enters the correlation function of the random potential.

We thus obtain a set of self-consistent equations for the $\tilde{s}_d(\omega)$'s and also $\tilde{s}(z)$ (or s_0 and s_1) at the same time and the Newton–Raphson method can be applied. When replica symmetry is not broken we simply obtain $u_c = 1$. The solution is then used (utilizing equation (5.4) of I) to calculate the sample-to-sample fluctuation of $\langle \boldsymbol{x}^2 \rangle$ as given in equation (3.10), and is depicted in figure 3.

References

[1] See Goldschmidt Y Y and Lai P Y 1990 *Phys. Rev. Lett.* **64** 2467 and references therein
[2] Wu W, Ellmann B, Rosenbaum T F, Aeppli G and Reich D H 1991 *Phys. Rev. Lett.* **67** 2076
Wu W, Bitko D, Rosenbaum T F and Aeppli G 1993 *Phys. Rev. Lett.* **71** 1919
[3] Sachdev S 1994 *Phys. World* **7** 25
[4] Miller J and Huse D 1993 *Phys. Rev. Lett.* **70** 3147
Ye J, Sachdev S and Read N 1993 *Phys. Rev. Lett.* **70** 4011
Read N, Sachdev S and Ye J 1995 *Phys. Rev.* B **52** 384
Hartman J W and Weichman P B 1995 *Phys. Rev. Lett.* **74** 4584
[5] Rieger H and Young A P 1994 *Phys. Rev. Lett.* **72** 4141
Guo M, Bhatt R N and Huse D 1994 *Phys. Rev. Lett.* **72** 4137
[6] Villain J *et al* 1983 *J. Phys. C: Solid State Phys.* **16** 2588
[7] Huse D A and Henley C L 1985 *Phys. Rev. Lett.* **54** 2708
Huse D A, Henley C L and Fisher D S 1985 *Phys. Rev. Lett.* **55** 2924
[8] Kardar M 1985 *Phys. Rev. Lett.* **55** 2923
Kardar M 1987 *Nucl. Phys.* B **290** 582
[9] Mézard M and Parisi G 1991 *J. Physique* I **1** 809
[10] Goldschmidt Y Y 1993 *Nucl. Phys.* B **393** 507
[11] Villain J 1988 *J. Phys. A: Math. Gen.* **21** L1099
[12] Schulz U, Villain J, Brézin E and Orland H 1988 *J. Stat. Phys.* **51** 1
[13] Mézard M and Parisi G 1992 *J. Physique* I **2** 2231
[14] Goldschmidt Y Y and Blum T 1993 *Phys. Rev.* E **48** 161
Goldschmidt Y Y and Blum T 1993 *Phys. Rev.* E **47** R2979
[15] Engel A 1993 *Nucl. Phys.* B **410** 617
[16] Goldschmidt Y Y 1994 *J. Physique* I **4** 87
Goldschmidt Y Y 1994 *J. Physique* I **4** 1583
[17] de Almeida J R L and Thouless D 1978 *J. Phys. A: Math. Gen.* **11** 983
[18] Binder K and Young A P 1986 *Rev. Mod. Phys.* **58** 801
[19] Goldschmidt Y Y 1995 *Phys. Rev. Lett.* **74** 5162
[20] Goldschmidt Y Y 1996 *Phys. Rev.* E **53** 343
[21] Goldschmidt Y Y 1996 *Preprint* University of Pittsburgh
[22] Nelson D R and Vinokur V M 1993 *Phys. Rev.* B **48** 13 060
[23] Feynman R P 1972 *Statistical Mechanics: A Set of Lectures* (New York: Benjamin)
[24] Takahashi M and Imada M 1984 *J. Phys. Soc. Japan* **53** 963
[25] Berne B J and Thirumalai D 1986 *Ann. Rev. Phys. Chem.* **37** 401
[26] Runge K and Chester G V 1988 *Phys. Rev.* B **38** 135
[27] Sprik M, Klein M L and Chandler D 1985 *Phys. Rev.* B **31** 4234
[28] Press W H, Teukolsky S A, Vetterling W T and Flannery B P 1992 *Numerical Recipes* 2nd edn (Cambridge: Cambridge University Press)